Supporting Information

Skin-Effect-Inspired 3D Solar Evaporator for Simultaneously Achieving Highly-Efficient Steam Generation and Ultra-High Salt Resistance

Renzhong Deng[1], Yunqi Li[1], Qing Li[*], Yu Qiu, Haixiang Feng, Yangming Liu

[1] These authors contributed equally to this work.

School of Energy Science and Engineering, Central South University, Changsha 410083, China.

[*] Corresponding author: Prof. Qing Li, email address: qingli@csu.edu.cn

1. Mechanical Strength Testing

The mechanical strength of SEISE was tested through a simple pressure test. A 500 g magnet was steadily placed on the top surface of SEISE (a height of 4 cm) for 1 min. Its height change was monitored. As shown in **Figure S1**, there was no significant change in the height of SEISE before and after the pressure test, indicating its superior mechanical strength.

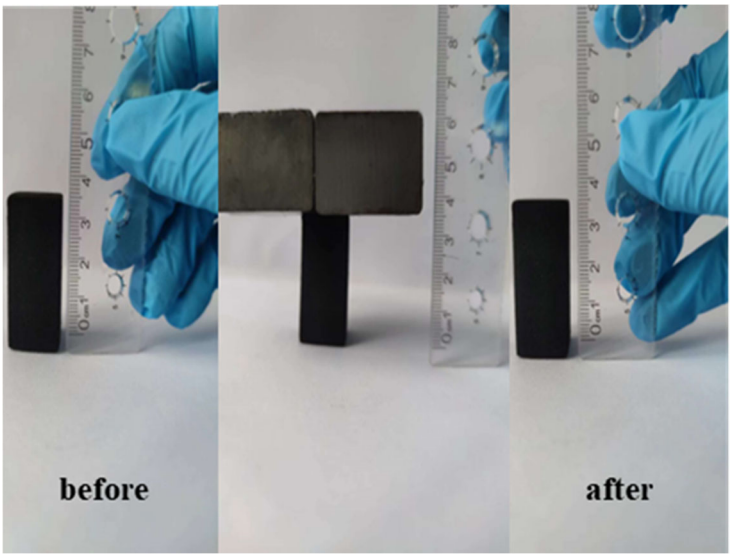

Figure S1. Mechanical strength testing of SEISE.

2. The Pore Structure of SEISE

To better illustrate the non-uniform porosity characteristics of SEISE, a comprehensive analysis was conducted using an automatic mercury porosimeter (Micromeritics Autopore V 9620, America), which can measure and compare the pore structures across different regions of SEISE. As shown in **Table S1**, the average pore size at the surface layer of SEISE is significantly smaller (about 473.62 nm) than that of the internal body of SEISE, which has an average pore size of 136.49 μm. This difference indicates a more compact pore structure at the surface layer compared to the internal body of SEISE. Furthermore, the total pore volume at the surface layer is 6.96 $mL \cdot g^{-1}$, which is considerably lower than that of the internal body of SEISE (90.44 $mL \cdot g^{-1}$). This shows that the internal body of SEISE contains a much larger volume of pores, likely contributing to its higher porosity. Conversely, the density of the surface layer (0.1276 $g \cdot mL^{-1}$) is much higher than that of the internal body (0.0108 $g \cdot mL^{-1}$) of SEISE. This difference in density can be attributed to the more compact pore structures and possibly higher solid material content at the surface layer of SEISE. To sum up, these findings confirm the non-uniform porosity of SEISE, with the surface layer exhibiting smaller pores, lower pore volume, and higher density than the internal body of SEISE.

Table S1. The pore structure of SEISE at different regions.

Sample types	Average pore size	Total pore volume ($mL \cdot g^{-1}$)	Density ($g \cdot mL^{-1}$)
Internal body	136.49 μm	90.44	0.0108
Surface layer	473.62 nm	6.96	0.1276

3. Evaporation Efficiency of SEISE

The evaporation efficiency of SEISE was calculated by **Equation S1** and **Equation S2**. As shown in **Figure S2**, the evaporation efficiency (η) of SEISE at a steady state was 168.10%.

$$\eta = \frac{M_r\left(C_p\Delta T + E\right)}{C_{opt}P_o} \tag{S1}$$

$$M_r = M_e - M_d \tag{S2}$$

Here M_r is the net evaporation rate of SEISE at a steady state, $kg\cdot m^{-2}\cdot h^{-1}$, C_p is the specific heat capacity of water (4.18 $kJ\cdot kg^{-1}\cdot K^{-1}$), ΔT is the temperature difference between the vapor and the environment, °C, E is the equivalent vaporization enthalpy of the water in SEISE, $kJ\cdot kg^{-1}$, C_{opt} refers to the optical concentration on the absorber surface, P_o is the solar irradiation power, $kW\cdot m^{-2}$, and M_e and M_d are the evaporation rates of SEISE at a steady state under 1 sun and dark condition ($kg\cdot m^{-2}\cdot h^{-1}$), respectively.

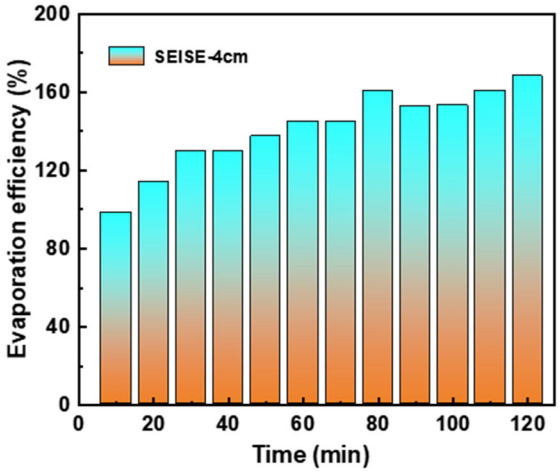

Figure S2. The evaporation efficiency of SEISE.

4. The Wetting State and Temperature Distribution

The traditional SE and SEISE were cut vertically to observe the wetting situation and temperature distribution of their cross-sections. As shown in **Figures S3a**, **S3b**, **S3c**, and **S3d**, the entire cross-section of the traditional SE was completely wetted by water, while only the surface layer of SEISE was wetted, and its internal body was still dry. Furthermore, as plotted in **Figures S3e**, **S3f**, **S3g**, and **S3h**, the average temperature of the traditional SE at the cross-section was higher than that of SEISE. Specifically, the highest and average temperatures within the marked area in the traditional SE's cross-section are 31.9 °C and 30 °C, respectively. However, for the marked area in the SEISE's cross-section, the highest and average temperatures are 29 °C and 27.9 °C, respectively. These results further prove that SEISE exhibits better thermal localization capacity.

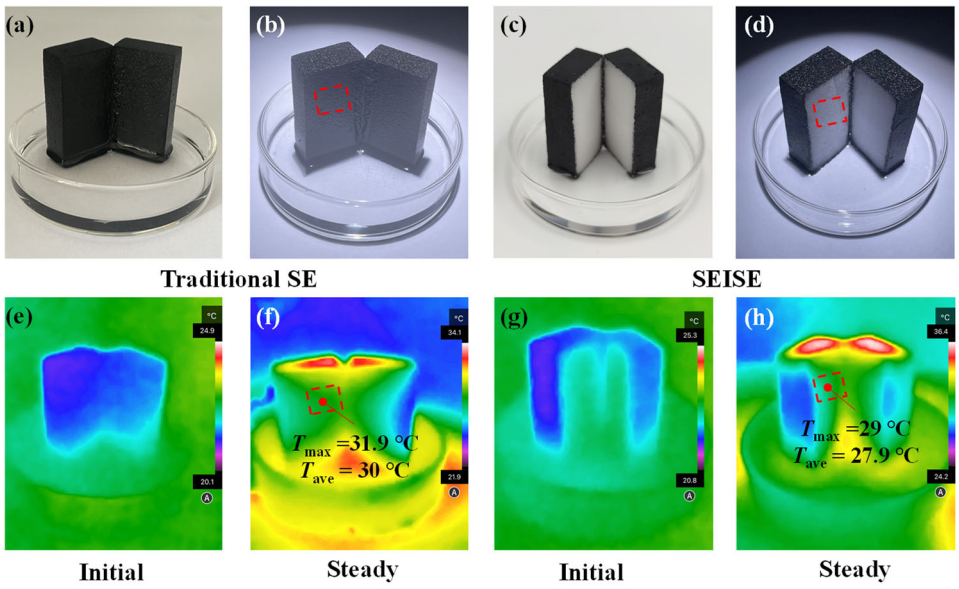

Figure S3. The entire wetting state (a, b, c, and d) and temperature distributions (e, f, g, and h) of traditional SE and SEISE at the cross-section.

5. The Long-term Stability Testing

To further evidence the long-term stability of SEISE, the evaporation rates of SEISE with different storage times (3 weeks or 2 months) were tested. As shown in **Figure S4**, the evaporation rates of SEISE remain basically unchanged after storage for a long time (the evaporation performance of the initial sample, sample storage for 3 weeks, and sample storage for 2 months was compared), indicating the excellent long-term stability of SEISE.

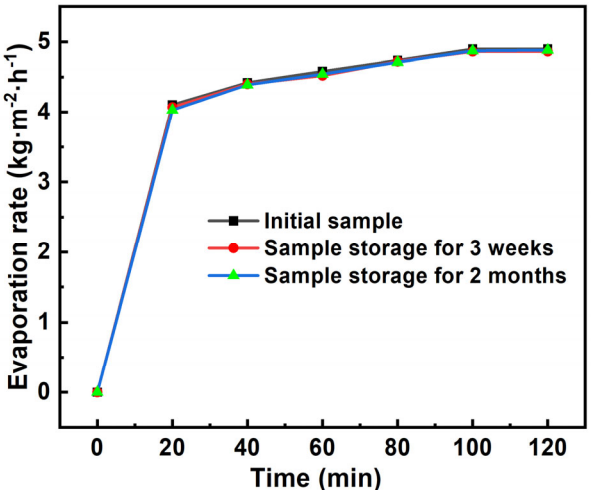

Figure S4. The evaporation performance of SEISE after storage for a long time.

6. The Water Absorption Capacity of SEISE at Different Regions

To further prove the localization of water transport in the surface layer of SEISE, SEISE was cut into pieces vertically with dimensions of 25×15×2.5 mm to weigh various portions to evaluate the water absorption capacity. As shown in **Figures S5a** and **S5b**, the front side of Sample 1 is the surface layer of SEISE, while Sample 2 is obtained from the internal body of SEISE. **Figure S5c** exhibits the weights of Sample 1 and Sample 2 at different states. At the dry state, the weights of Sample 1 and Sample 2 are 33.1 mg and 10.4 mg, respectively. At the working state, the weight of Sample 1 increases to 299.8 mg, while the weight of Sample 2 just rises to 26.4 mg. Sample 1 exhibits a high water-absorption of 266.7 mg, which is significantly higher than that of Sample 2 (16.0 mg). The water absorption rate of Sample 1 is approximately 5.11 times that of Sample 2. To sum up, this substantial difference in the water absorption between the two samples indicates that the water in Sample 1 is predominantly absorbed by the low porosity surface structure located at its front side.

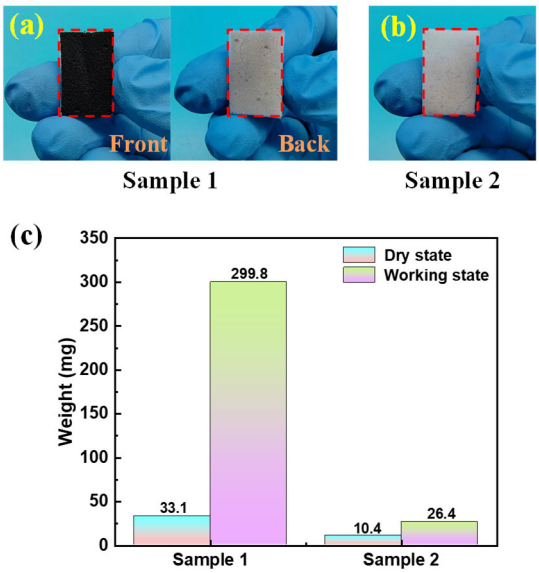

Figure S5. The images of Sample 1 (a) and Sample 2 (b). (c) The weights of Sample 1 and Sample 2 at the dry state and working state.

7. The Contact Angle of SEISE

The contact angle of SEISE was measured by a contact angle meter (**Figure S6**). It can be seen that a microdroplet (10 μL) is rapidly absorbed by the surface of SEISE within 0.1 s, with a contact angle of approximately 0° (similar to the test results in Refs. [1-3]), showing the excellent wettability of SEISE.

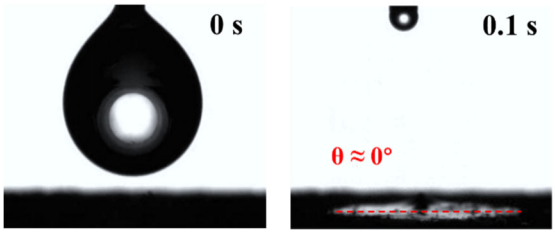

Figure S6. The contact angle test of SEISE.

8. Interfacial Evaporation Experiment Device

Figure S7 exhibited the digital photo of the interfacial evaporation experiment device, including a solar simulator, an electronic balance, a computer, a thermo-hygrometer, and a break-wind.

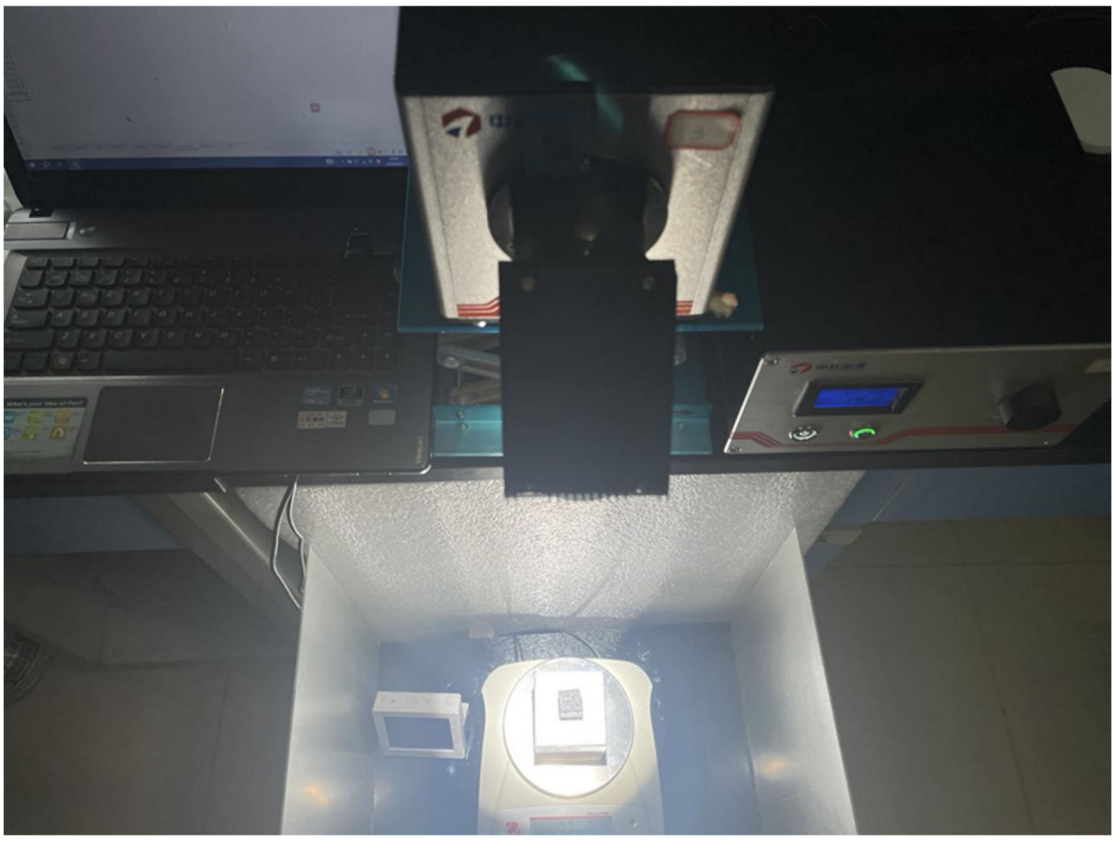

Figure S7. The digital photo of the interfacial evaporation experiment device.

References

[1] Lei Z, Zhu S, Sun X, Yu S, Liu X, Liang K, et al. A Multiscale Porous 3D-Fabric Evaporator with Vertically Aligned Yarns Enables Ultra-Efficient and Continuous Water Desalination. Advanced Functional Materials, 2022, 32(40):

[2] Jing M, Wang W, Fu Y, Yang Y, Song W, Sun Z. A simple, natural 3D honeycomb structure achieving high photothermal conversion and sustainable salt-resistance for efficient desalination and potential electricity generation. Desalination, 2023, 564: 116792.

[3] Zhu J, Chen X, Zhang C, Cui B, Bai N, Wang W, et al. Biopolymer Hydrogel-Based Salt-Resistant Evaporator for Solar-Energy-Driven Desalination and Water Purification. Langmuir, 2024, 40(21): 11317-11328.